

Structural Instability and Fibrillar Aggregation of Non-expanded Human Ataxin-3 Revealed under High Pressure and Temperature*

Received for publication, April 22, 2003, and in revised form, May 20, 2003
Published, JBC Papers in Press, May 23, 2003, DOI 10.1074/jbc.M304205200

Stéphane Marchal‡, Erlet Shehi§, Marie-Cécile Harricane¶, Paola Fusi§, Frédéric Heitz¶, Paolo Tortora§, and Reinhard Lange‡||

From ‡INSERM U128, IFR 122, 1919 route de Mende, F-34293 Montpellier Cédex 5, France, §Dipartimento di Biotecnologie e Bioscienze, Università di Milano-Bicocca, Piazza della Scienza 2, I-20126 Milano, Italy, and ¶Centre de Recherches de Biochimie Macromoléculaire, Formation de Recherche en Evolution 2953, Institut Fédératif de Recherche 122, 1919 route de Mende, F-34293 Montpellier Cédex 5, France

Protein misfolding and formation of structured aggregates are considered to be the earliest events in the development of neurodegenerative diseases, but the mechanism of these biological phenomena remains to be elucidated. Here, we report a study of heat- and pressure-induced unfolding of human Q26 and murine Q6 ataxin-3 using spectroscopic methods. UV absorbance and fluorescence revealed that heat and pressure induced a structural transition of both proteins to a molten globule conformation. The unfolding pathway was partly irreversible and led to a protein conformation where tryptophans were more exposed to water. Furthermore, the use of fluorescent probes (8-anilino-1-naphthalenesulfonate and thioflavin T) allowed the identification of different intermediates during the process of pressure-induced unfolding. At high temperature and pressure, human Q26, but not murine Q6, underwent concentration-dependent aggregation. Fourier transform infrared and circular dichroism spectroscopy revealed that these aggregates are characterized by an increased β -sheet content. As revealed by electron microscopy, heat- and pressure-induced aggregates were different; high temperature treatment led to fibrillar microaggregates (8–10-nm length), whereas high pressure induced oligomeric structures of globular shape (100 nm in diameter), which sometimes aligned to higher order suprastructures. Several intermediate structures were detected in this process. Two factors appear to govern ataxin unfolding and aggregation, the length of the polyglutamine tract and its protein context.

Polyglutamine (polyGln)¹ diseases are autosomal-dominant neurodegenerative disorders caused by aggregation of proteins containing expanded polyGln sequences, with concomitant formation of insoluble β -sheet-rich fibrils (1–3). In turn, expansion of polyGln tract results from instability of the encoding trinucleotide (CAG) repeats (1, 4, 5). Spinocerebellar ataxia types 1, 2, 3, 6, and 7 and Huntington's disease belong to this

superfamily of polyglutamine-associated diseases. Among these, an expanded polyGln tract located at the C-terminal part of the 42-kDa ataxin-3 protein triggers spinocerebellar ataxia type-3 (SCA3), also known as Machado-Joseph disease (MJD). The repeat normally consists of 15–30 consecutive glutamines, whereas up to 55–84 glutamines are found in pathological variants (6). The expansion of the glutamine repeat destabilizes the native α -helix-rich protein, which aggregates into amyloid-like β -fibrils (7). This event is considered to play a crucial role in early pathological steps leading to the disease (8–10).

However, the normal, non-expanded form of ataxin-3 also appears to be involved in aggregation processes. Indeed, recent studies (11–13) showed intranuclear aggregation of ataxin-3 in marinesco bodies in human and non-human primate substantia nigra. It has also been hypothesized that the pathogenic effects of marinesco bodies could be because of these aggregates (14, 15). Chai *et al.* (16) found nuclear inclusions containing normal ataxin-3. This led them to postulate that not only the polyGln tract, but also other parts of the protein, are involved in the aggregation mechanism. Moreover, an ill-folded conformation of ataxin-3 where the glutamine domain is solvent-exposed could represent the starting point of neuronal dysfunction in SCA3/MJD, as suggested by Perez *et al.* (17). These observations prompted us to study and examine the role of the polyGln chain length and its protein environment on structural stability and aggregate formation of normal, non-pathologic ataxin-3.

In the present study, we used as models a non-pathological variant of human ataxin-3, which includes a tract of 26 consecutive glutamines (Q26), and its murine counterpart, which has only six residues (Q6). These proteins display high sequence homology (Fig. 1) with 99% identity in the N-terminal part, called Josephin domain. The C-terminal region is more divergent. A three-dimensional structural model of ataxin-3 has been proposed recently (18), suggesting a common structure for the two proteins. To study the mechanism of ataxin-3 structural changes and aggregation, we used heat and pressure as thermodynamic perturbants. Whereas heat is widely used as a structure perturbing agent, high pressure techniques are not applied extensively. Nonetheless, hydrostatic pressure, in combination with spectroscopic methods, is a powerful tool to study protein structural changes, such as folding-unfolding, oligomer dissociation equilibrium, and aggregation (19–31). This is because of its specific effects on non-covalent interactions. Indeed, this property sometimes facilitates trapping of thermodynamically stable intermediates. In contrast, application of high temperature or treatment by chemical denaturants often

* This research was supported by the Human Science Frontier Program, and by Telethon, Italy Project 1021. The costs of publication of this article were defrayed in part by the payment of page charges. This article must therefore be hereby marked "advertisement" in accordance with 18 U.S.C. Section 1734 solely to indicate this fact.

|| To whom correspondence should be addressed. Tel.: 33-467-61-33-65; Fax: 33-467-52-36-81; E-mail: lange@montp.inserm.fr.

¹ The abbreviations used are: polyGln, polyglutamine; FTIR, Fourier transform infrared spectroscopy; ANS, 8-anilino-1-naphthalenesulfonate; ThT, thioflavin T; SCA3, spinocerebellar ataxia type-3; MJD, Machado-Joseph disease; MPa, megapascal.

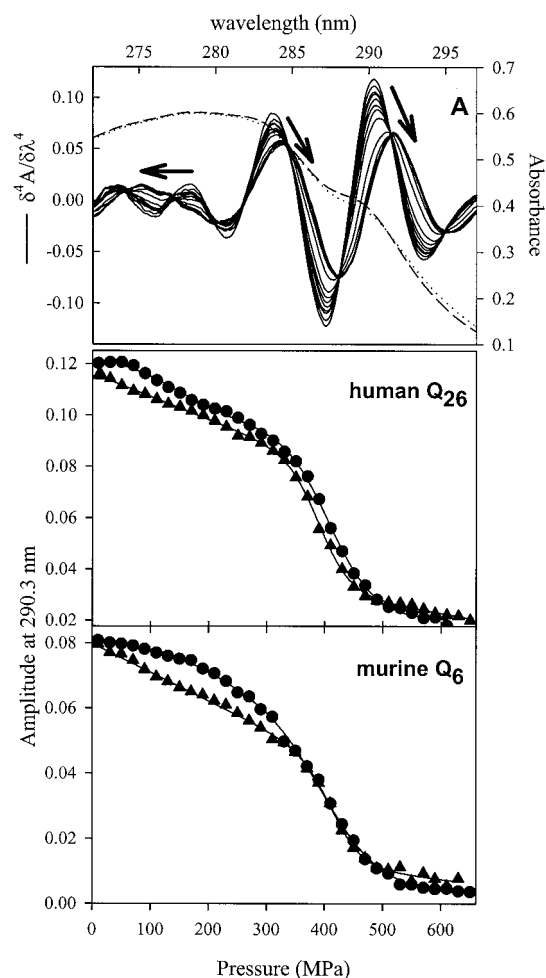


FIG. 2. Effect of hydrostatic pressure on stability of ataxin-3 shown by UV spectroscopy at 25 °C. Upper graph, representative view of fourth derivative UV spectra of human Q26 ataxin-3 as a function of hydrostatic pressure between 0.1 and 650 MPa. Protein concentration was 1.5 mg·ml⁻¹ in 25 mM Tris-HCl buffer, pH 7.0. Pressure was raised in steps of 20 MPa from 0.1 to 650 MPa. Only intervals of 60 MPa are shown. For a comparison, shown are the original zero order spectra at 0.1 MPa of the human (dashed line) and murine (dotted line) proteins (right hand scale). Middle and bottom graphs, effects of salts on the fourth derivative amplitude in the tryptophan region corresponding to pressure unfolding of the human and murine proteins in the absence (●) and in the presence of 1 M NaCl (▲). Data were the average (S.D. ± 5%) of three independent experiments. Solid lines are the nonlinear least squares fit of experimental against a two or multi-state model, as specified under “Results.”

mined by fitting spectral amplitudes at characteristic wavelengths to two- or three-state transitions as described (22). This was possible, because under each condition microreversibility was attained (the spectra did not change further as a function of time). Nevertheless, the pressure- and temperature-dependent spectral changes were not always fully reversible, and in some cases (as specified under “Results”) a hysteresis phenomenon was observed. The deduced thermodynamic parameters are therefore meaningful only within our experimental conditions. They are used to compare the stability of murine and human ataxin-3.

Circular Dichroism Spectroscopy—CD spectra were performed on a Jasco model 810 polarimeter. 0.1- and 0.5-cm optical path length quartz cells were used, respectively, to record spectra in the far-UV (188–260 nm) and near-UV (250–300 nm) range. Baseline corrected spectra were acquired in triplicate at a scan speed of 20 nm·min⁻¹, using a bandwidth of 1 nm with a response time of 1 s. For temperature experiments in the far-UV and near-UV ranges, proteins were dissolved at concentrations of 0.24 and 1.2 mg·ml⁻¹, respectively, in 25 mM phosphate buffer, pH 7. Spectra were recorded in steps of 5 °C from 25 to 90 °C. At each temperature the solution was allowed to equilibrate for 15 min.

FTIR Spectroscopy—FTIR spectra were recorded with an IFS28 spectrometer equipped with a DTGS detector. The spectra resulted from an

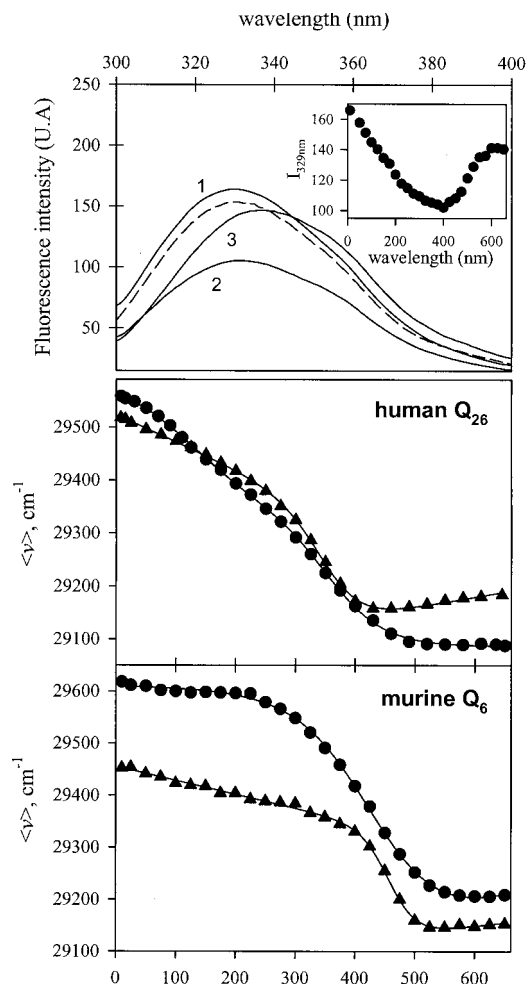


FIG. 3. Pressure effect on the intrinsic protein fluorescence of ataxin-3 at pH 7 and 25 °C. Upper graph, representative view of fluorescence emission spectra of murine Q6 upon excitation at 280 nm as a function of hydrostatic pressure at 0.1 MPa (1), 300 MPa (2), and 650 MPa (3) and after decompression (dashed line). Inset, variation of the maximal value of fluorescence intensity ($I_{329\text{nm}}$) as a function of increasing pressures. Middle and bottom graphs, effect of salts on the pressure dependence of the center of spectral mass $\langle v \rangle_3$ for human Q26 and murine Q6 proteins in the absence (●) and in the presence of 1 M NaCl (▲). Data were the average (S.D. ± 5%) of three independent experiments. Solid lines are the nonlinear least squares fit of the data on a two- or multi-state model, as stated under “Results.”

accumulation of 100 scans, which were collected at a resolution of 2 cm⁻¹. To compare soluble and aggregated proteins, spectra were recorded with dry samples. Aliquots were applied onto fluorine plates, and the solvent was allowed to evaporate at room temperature. For comparison, spectra were normalized using the program OPUS/IR2.

Electronic Microscopy—Aggregates were obtained by pressurization (650 MPa) or heating (90 °C) of human Q26 ataxin-3 protein solution at 2 mg·ml⁻¹. The aggregates were diluted to a protein concentration of 0.2 mg·ml⁻¹, deposited onto formvar-carbon-coated grids, and negatively stained with 2% aqueous uranyl acetate. The grids were examined using a JEOL 1200EX² electron microscope at an accelerating voltage of 80 kV.

RESULTS

Pressure-induced Unfolding Studies using UV Absorbance and Intrinsic Protein Fluorescence Show a More Complex, Multi-step Unfolding Mechanism for Q26 Ataxin-3, as Compared with That of the Q6 Form—At atmospheric pressure, human Q26 and murine Q6 ataxin-3 exhibited identical UV absorption and fluorescence spectra at pH 7.4 and 25 °C (see Figs. 2 and 3). To compare the conformational stability of the two proteins, pressure-induced unfolding experiments were

TABLE I
Thermodynamic parameters calculated from pressure and temperature unfolding curves of ataxin-3 at 25 °C

	Pressure			Temperature	
	ΔV <i>ml·mol⁻¹</i>	ΔG_U <i>kJ·mol⁻¹</i>	$P_{1/2}$ <i>MPa</i>	$T_{1/2}$ <i>°C</i>	ΔG_U^a <i>kJ·mol⁻¹</i>
Human Q26					
Absorbance	$-40.7 \pm 3.9_{(1)}^b$	$5.9 \pm 0.7_{(1)}^b$	$145_{(1)}^b$	47.8 ± 0.5	12.7
Absorbance + 1M NaCl	$-61.3 \pm 1.9_{(2)}^b$	$25.0 \pm 0.8_{(2)}^b$	$409_{(2)}^b$		
Fluorescence	$-37.2 \pm 5.4_{(1)}^b$	$4.6 \pm 0.5_{(1)}^b$	$123_{(1)}$	49.9 ± 0.4	20.5
Fluorescence + 1M NaCl	$-50.5 \pm 3.2_{(2)}^b$	$17.8 \pm 1.4_{(2)}^b$	$352_{(2)}$		
Near-UV CD	-69.9 ± 3.4	24.7 ± 1.2	353	49.2 ± 0.1	20.9
Murine Q6					
Absorbance	-36.9 ± 1.1	13.5 ± 0.5	366	55.3 ± 0.6	7.0
Absorbance + 1M NaCl	-91.8 ± 8.0	38.3 ± 3.2	417		
Fluorescence	-47.1 ± 2.2	19.6 ± 0.9	416	53.8 ± 0.3	10.5
Fluorescence + 1M NaCl	-104.9 ± 6.9	48.2 ± 3.1	459		
Near-UV CD				53.1 ± 0.5	8.3

^a Free energy of heat-induced unfolding determined at 25 °C.

^b The parameters were deduced from nonlinear regression of pressure-induced unfolding (Figs. 2 and 3) according to a bisigmoid model.

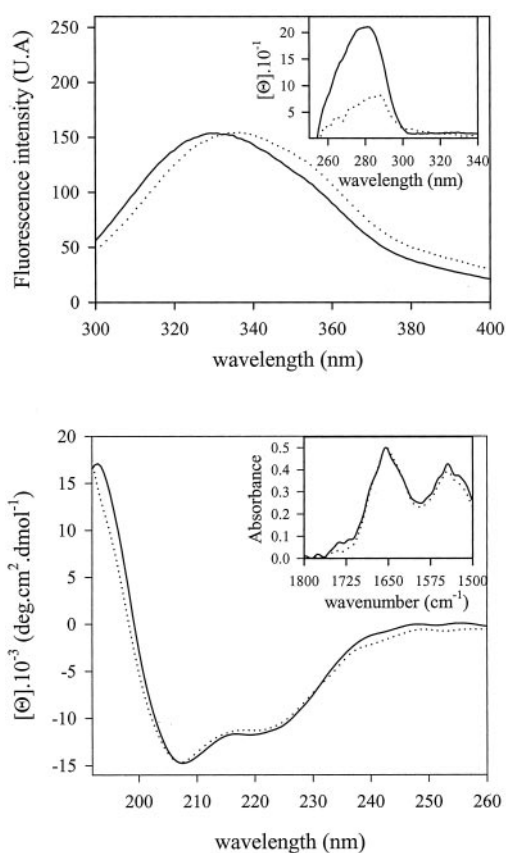


FIG. 4. Pressure-induced effects on secondary and tertiary structures of human Q26 ataxin-3. Upper graph, fluorescence emission spectra before (solid line) and after (dotted line) pressure treatment. Inset, corresponding near-UV CD analysis. Bottom graph, far-UV CD and infrared (inset) spectra of intact and pressurized protein (solid and dotted lines, respectively). Similar effects were observed for the murine Q6 protein (not shown for clarity).

performed under the same conditions. Using fourth derivative UV absorbance spectroscopy, significant spectral changes were observed for human Q26 and murine Q6 ataxin-3. As shown in Fig. 2, increasing pressure up to 650 MPa induced a red shift from 290.5 to 291.7 nm in the area corresponding to tryptophan residues. Taking the spectral amplitude at 290.3 nm as the signal of the transition, the change of the fourth derivative value with pressure exhibited a sigmoid profile for the murine

protein (Fig. 2). This conformational destabilization was characterized by a free energy of unfolding, $\Delta G_U = 13.5$ kJ/mol, and a standard volume change of $\Delta V = -36.9$ ml/mol with a half-transition pressure, $P_{1/2}$, of 366 MPa (Table I). The analysis of the corresponding profile for the human Q26 ataxin-3 was more complicated; the presence of an intermediate was required to accurately fit the experimental data (Fig. 2) as suggested by the residuals of the global fit (data not shown). This yielded values of ΔG_U of 5.9 and 25 kJ/mol and ΔV of -40.7 and -61.3 ml/mol, with $P_{1/2}$ values of 145 and 409 MPa (Table I). Although reversibility was attained at each pressure (no further spectral evolution as a function of time), for both proteins the spectral change attained at 650 MPa was not fully reversible. After pressure release, their spectra did not return to their initial levels, as indicated by the incomplete recovery of the pressure-induced red shift of the tryptophan band from 291.7 (650 MPa) to 291 nm (10 MPa).

The effect of hydrostatic pressure on ataxin-3 fluorescence spectra is shown in Fig. 3. For the murine Q6, the protein fluorescence is affected in two phases in the pressure range from 10 to 650 MPa (Fig. 3, inset). From 10 to 300 MPa, a gradual decrease in fluorescence intensity at 329 nm was observed upon compression. At higher pressure, the fluorescence intensity increased. Concomitantly with the fluorescence intensity increase, a red shift of the maximum emission wavelength was observed, indicative of a pressure-dependent exposure of tryptophan residues to water. These spectral changes were not fully reversible. In the case of human Q26, the fluorescence intensity changed in a similar way as that of murine Q6. However, the pressure-dependent red shift was observed already in the low pressure range. Again, these spectral changes were only partly reversible; as illustrated in Fig. 4, the maximum of fluorescence intensity after pressure release was red-shifted. This indicates that the tryptophan residues became more exposed to water. The partly irreversible character of the unfolding process was confirmed by a significant decrease of the near-UV CD signal (Fig. 4). However, far-UV CD and infrared spectra were identical before and after compression (Fig. 4). Altogether, these results indicate that the pressure-induced unfolding process did not change irreversibly the protein secondary structure but modified their tertiary structure. For the murine Q6, the transition can be ascribed to a two-state model, whereas at least three states are involved in the pressure-dependent unfolding of the human Q26 protein (Fig. 3). The calculated thermodynamic parameters are listed in Table I.

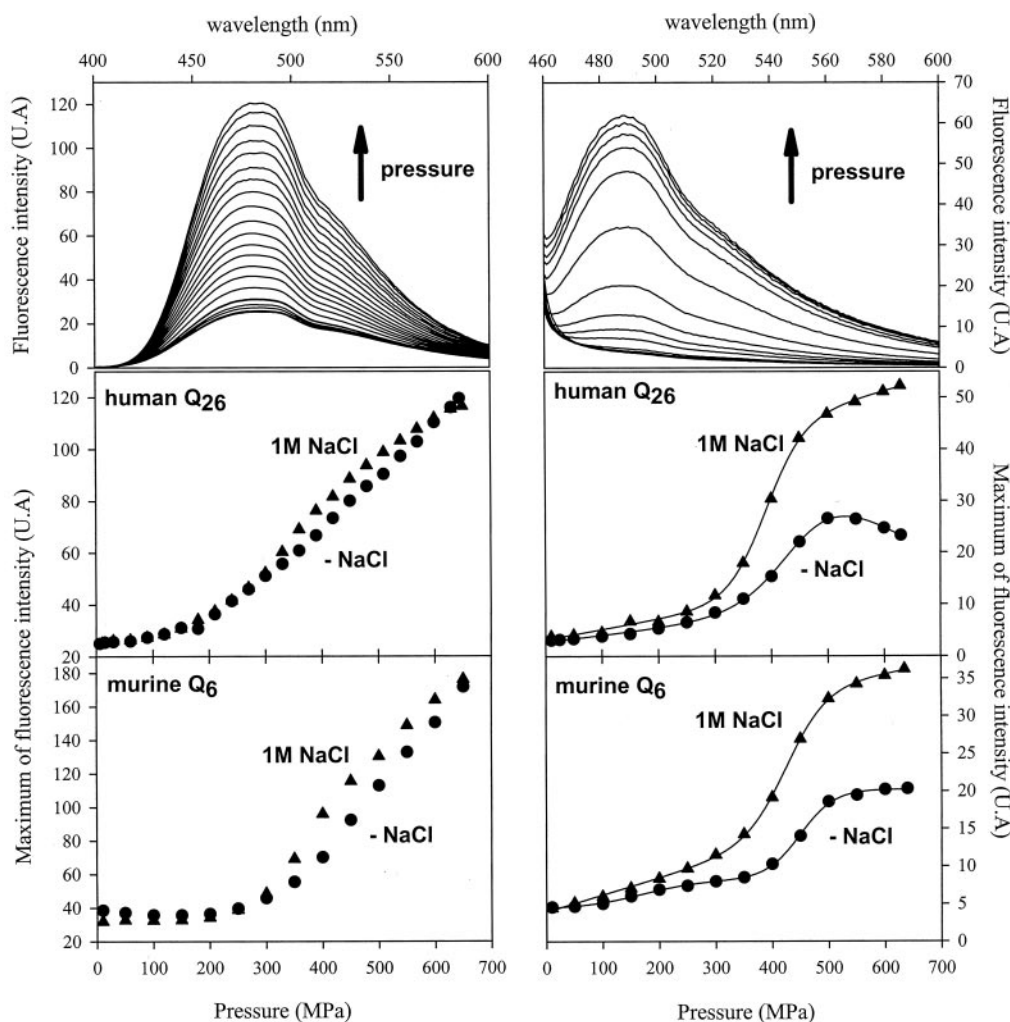


FIG. 5. Binding of ANS (left) and thioflavin T (right) on pressure-unfolded ataxin-3 proteins at pH 7 and 25 °C. Left, upper graph, fluorescence emission spectra reflecting ANS binding to ataxin-3 (case of human Q26) as a function of pressure between 0.1 and 650 MPa. The arrows indicate the change in fluorescence intensity of the probes with increasing pressure from 10 to 650 MPa. Middle and bottom graphs, pressure dependence of fluorescence intensity for the binding of ANS in the absence (●) and in the presence of 1 M NaCl (▲) for the human and murine proteins. Right, upper graph, fluorescence emission spectra reflecting ThT binding to ataxin-3 (case of human Q26) as a function of pressure between 0.1 and 650 MPa. Middle and bottom graphs, effect of salt on the binding of ThT for the human Q26 or murine Q6 ataxin-3 protein in the absence (●) and in the presence of 1 M NaCl (▲). Data were the average (S.D. \pm 5%) of three independent experiments.

TABLE II
Thermodynamic parameters calculated from pressure-induced ThT binding curves for ataxin-3 at 25 °C and 0.1 MPa

	ΔV <i>ml·mol⁻¹</i>	ΔG_U <i>kJ·mol⁻¹</i>	$P_{1/2}$ <i>MPa</i>
Human Q26	-53.3 ± 3.9	23.9 ± 1.5	447
Human Q26 + 1 M NaCl	-71.7 ± 5.2	27.9 ± 2.0	390
Murine Q6	$-45.2 \pm 4.9_{(1)}^a$	$7.6 \pm 0.9_{(1)}^a$	$168_{(1)}^a$
	$-80.5 \pm 6.9_{(2)}^a$	$36.2 \pm 3.2_{(2)}^a$	$450_{(2)}^a$
Murine Q6 + 1M NaCl	-67.0 ± 4.6	28.6 ± 1.8	423

^a The parameters were deduced from nonlinear regression of Fig. 4 experimental data, according to a bisigmoid model.

NaCl Abolishes the Biphasic Denaturation Profile of Human Q26 Ataxin-3—To determine whether salts affect the stability of proteins as described previously (37) for murine prion protein, UV absorbance and fluorescence experiments were carried out in the pressure range from 0.1 to 650 MPa in the presence of 1 M NaCl. For human Q26, the former double-sigmoid UV absorbance and fluorescence profiles became two-state transitions, preceded and followed by near-linear slopes (see Figs. 2 and 3). The thermodynamic parameters (Table I) indicate that NaCl did not affect the unfolding process at high pressure (300–650 MPa). These results sug-

gest a destabilization by NaCl of one region of the protein at low pressure. In contrast, a pronounced increase in stability of the murine Q6 protein was observed under pressure; the presence of 1 M NaCl induced an increase of $P_{1/2}$ by about 50 MPa for both absorbance and fluorescence pressure-dependent profiles (Table I).

8-Anilino-1-naphthalenesulfonate and Thioflavin T Binding Fluorescence—The environment-sensitive fluorescent dye ANS was used to characterize the pressure-induced unfolding of ataxin-3. ANS binds to water-exposed hydrophobic domains of native or molten globule protein structures (25, 31, 38, 39). ANS binding is accompanied by an increase in its fluorescence quantum yield. We used this probe to follow pressure-induced exposure of hydrophobic regions of ataxin-3 proteins. As shown in Fig. 5, ANS fluorescence intensity increased with hydrostatic pressure for both proteins. In the experimentally available pressure range, no plateau was attained, indicating that the pressure-induced structural changes were incomplete even at 650 MPa. Again, this process was only partially reversible. Comparing the two proteins, ANS bound to human Q26 at lower pressure than to murine Q6 (100 and 250 MPa, respectively) indicating that the human protein is less resistant to pressure treatment.

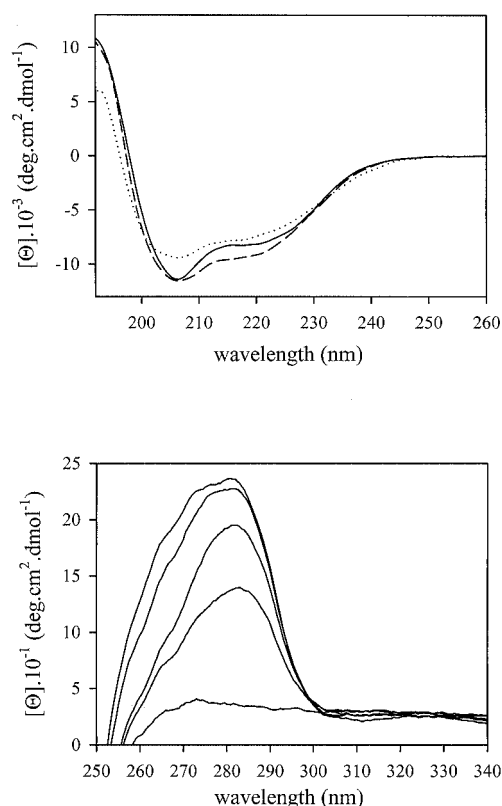


FIG. 6. Far- (top) and near-UV (bottom) CD analysis as a function of temperature for the murine Q6 ataxin-3. For the far-UV CD, only the spectra at extreme temperatures (solid line, 25 °C; dotted line, 90 °C) and the spectrum recorded after cooling to 25 °C (dashed line) are shown.

For a further characterization of the pressure-induced conformational states, the ability of ataxin-3 to bind ThT was studied. This fluorophore is frequently used to detect amyloid (40) or oligomeric protein structures (41). Under our conditions, its binding was characterized by a fluorescence increase at 483 nm (Fig. 5). For the human Q26 protein, a plot of the emission amplitude at 483 nm *versus* pressure was best fitted by a two-state transition model, whereas a multi-step process described the profile obtained for the murine counterpart (Fig. 5). This process was completely reversible with hysteresis in the pressure range from 400 to 200 MPa. The thermodynamic parameters deduced from these profiles are listed in Table II. ThT binding was also observed in the presence of 1 M NaCl. The observed sigmoid profiles were characterized by similar values of ΔG_U , ΔV , and $P_{1/2}$ for both proteins (see Fig. 5 and Table II).

Thermal Unfolding of Ataxin-3—In contrast to pressure-induced unfolding, human Q26 and murine Q6 showed similar behavior against temperature. Fourth derivative spectra of the tryptophan bands and protein fluorescence showed irreversible red shifts at high temperature (data not shown). To obtain a more detailed picture of their thermal unfolding, we analyzed their CD spectra in the far- and near-UV range. (Fig. 6). In the 188–260-nm range, limited spectral changes were observed when temperature was increased from 25 to 90 °C (Fig. 6A). Again, the process was reversible after cooling to 25 °C. In contrast, the CD signal at 282 nm decreased until complete disappearance at 75 °C for the murine Q6 (Fig. 6B) and human Q26 protein (data not shown). The temperature dependence of the molar ellipticity at 282 nm exhibited a sigmoidal profile superimposable to that obtained by absorbance and fluorescence experiments for both proteins (Fig. 7). The temperature-induced unfolding parameters are reported in Table I.

Temperature- and Pressure-dependent Aggregation of Hu-

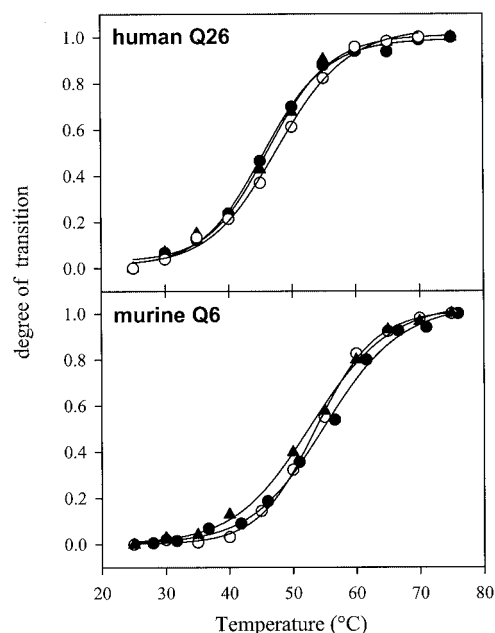


FIG. 7. Temperature-induced unfolding as measured by absorption, fluorescence, and near-UV circular dichroism. The degree of the transition was calculated from the fourth derivative amplitude at 290.3 nm (●), the shift of the center of spectral mass (▲), and near-UV CD signal at 282 nm (○) as a function of temperature for the human Q26 and murine Q6 ataxin-3. For absorbance and fluorescence experiments, experimental conditions were identical to those used for pressure treatment, except that the buffer was 25 mM phosphate, pH 7.0. For near-UV CD analysis, the spectra were recorded by increments of 5 °C from 25 to 70 or 75 °C for the human and murine proteins (for further information, see “Results”). The solid lines represent the fitting of data using nonlinear regression against a two-state transition model.

man Ataxin-3—Human Q26, but not murine Q6, was prone to aggregation at high pressure and temperature when its concentration was raised to 2 mg·ml⁻¹ (Fig. 8). Interestingly, the aggregation process occurred in the same pressure range as the second transition of the pressure-induced unfolding in fluorescence experiments. The corresponding profile could be fitted by a two-state model with a similar half-transition value, $P_{1/2}$, like that determined from fluorescence data (352 and 371 MPa, respectively). The aggregates persisted during depressurization to atmospheric pressure. Irreversible protein aggregation was also observed at high temperature. In the case of murine Q6, no aggregation was observed at protein concentrations up to 3 mg·ml⁻¹ by pressure and temperature treatments.

The fact that ANS fluorescence and far-UV CD data suggest a partially folded conformational state of human Q26 at high pressure and temperature led us to examine the nature and the morphology of these aggregates. The secondary structures of soluble and aggregated proteins were determined by Fourier transform infrared spectroscopy. As shown in Fig. 8B, soluble protein before or after pressurization and pressure-induced aggregates have similar infrared spectra in the amide I band with an absorbance maximum at 1,654 cm⁻¹. No significant conformational changes in secondary structure were observed, thus suggesting unlikely any effect of drying samples on FTIR spectra. The only difference was the appearance of a minor shoulder at 1,640 cm⁻¹ for the aggregated protein. In contrast, a new peak showed up at 1,629 cm⁻¹ for the heat-aggregated protein, indicating that heat-induced aggregated Q26 contains more β -secondary structure than the pressure-induced aggregated protein.

Electron micrographs of negatively stained proteins revealed a strong difference in the morphology of pressure- and temperature-induced aggregates (Fig. 9). Surveying the en-

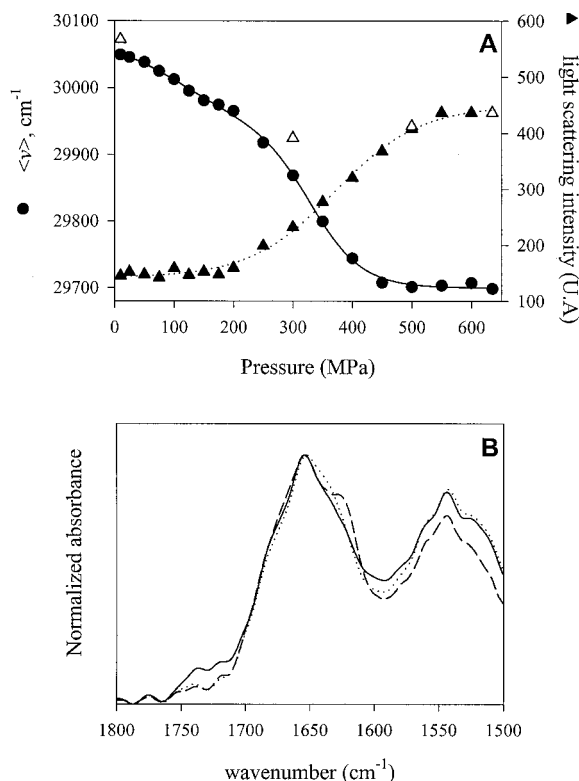


FIG. 8. Evidence of distinct structural and morphological intermediates of human Q26 ataxin-3 aggregates. A, pressure-induced aggregation of proteins monitored by light scattering at 350 nm and at 25 °C (\blacktriangle , compression; \triangle , decompression). For comparison, the profile corresponding to the change in the center of spectral mass $\langle v \rangle$ as a function of pressure has been included in the graph. The protein concentration was 2 $\text{mg}\cdot\text{ml}^{-1}$ in 50 mM Tris-HCl buffer, pH 7.0, for both experiments. Data were the average (S.D. \pm 5%) of three independent experiments. The *solid* and *dotted lines* are the nonlinear least squares fit of the data to a two- or multi-state model. B, infrared spectra of intact protein (*solid line*), after pressure (*dotted line*) or temperature treatment (*dashed line*).

tire electron micrograph grid, pressure-induced aggregation exhibited distinct structural conformers of human Q26 protein (Fig. 9A). Pressure treatment resulted into the simultaneous presence of unstructured aggregates, of spheroid structures (100 nm in diameter; *left*), and of superstructures of these spheroids to protofibrils of various length and order (*right*). In some cases, these short fibrils associated (*bottom*). In contrast, the picture was different for the temperature-induced aggregates. As shown in Fig. 9B, only small isolated filaments with a length of 8–10 nm were detected, without any higher order structure. In both cases, the aggregates did not exhibit birefringence in polarized microscopy after staining by Congo red, suggesting that no amyloid fibril formation took place during aggregation.

DISCUSSION

It is well known that an expansion of the polyGln stretch from 27 to 78 residues destabilizes ataxin-3 and leads to the formation of amyloid β -fibrils (7). However, little information is available concerning the stability and possible aggregation mechanism(s) of normal ataxin-3, whose polyGln length ranges from 12 to 40 (42). By using human and murine ataxin-3, which contain a sequence of 26 and six consecutive glutamines, respectively, we were able to compare directly the behavior of these orthologous proteins under pressure and temperature to determine the role of the polyglutamine sequence and its protein environment on the conformational stability and aggregation of ataxin-3.

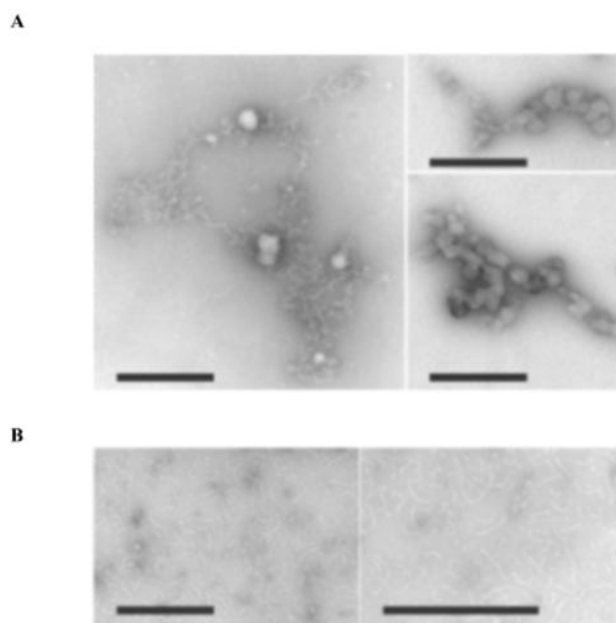


FIG. 9. Evidence for distinct morphological and structural intermediates in human Q26 ataxin-3 aggregation induced by pressure (A) or temperature (B). Aggregates were obtained after compression at 650 MPa or heating to 90 °C of the protein at a concentration of 2 $\text{mg}\cdot\text{ml}^{-1}$. A 10-fold dilution was applied on formvar-carbon-coated grids, and aggregates were imaged using a JEOL 1200EX² electron microscope. A, $\times 50,000$ (*bar*, 200 nm); B, $\times 50,000$ (*left*) and $\times 80,000$ (*right*) (*bar*, 200 nm).

Comparison of Fluorescence and Absorbance Results—At high temperature and high pressure, both proteins unfold. This is evidenced by the red shift of intrinsic fluorescence (indicating an increased water exposure of tryptophans), as well as by the increase of extrinsic ANS fluorescence, by the decrease of the near-UV CD signal, and by the blue shift of the tyrosine band at 278 nm of the fourth derivative UV absorbance spectra (Fig. 2). In contrast, the tryptophan band in the fourth derivative UV spectra (290.3 nm) shifts to the red. Commonly, such a red shift is ascribed to a less polar environment (19, 33). However, ataxin-3 may be an exception for this general rule (43). First, the absorbance profiles match the fluorescence profiles. Second, we have shown in tryptophan model studies that, unlike tyrosines, there is no linear relationship between the position of the absorbance band of tryptophan and the dielectric constant of the solvent. In contrast, the intensity of the tryptophan fourth derivative band has been shown to relate directly to the solvent polarity (32, 33). Indeed, on increasing temperature and pressure, the amplitude of the 290.3-nm band decreases, thus providing evidence for the increased water exposure of the tryptophans. A hypothesis to explain this result could be the enhancement of nonspecific interactions between water and one or more of the three tryptophans with increasing pressure, depending on their degree of solvent exposure (44). At 600 MPa the water density is 15% higher than at 0.1 MPa and, as a consequence, could favor the stabilization of the excited state of tryptophan(s). This would also explain the increase of tryptophan fluorescence intensity at high pressure (Fig. 3, *inset*).

Distinct Effects of Heat and Pressure upon Unfolding and Aggregation—As already observed with other proteins (31, 45, 46), heat and pressure induced different ataxin-3 unfolding processes. As to heat, the unfolding profiles of human Q26 and murine Q6 were similar; they reflected a two-state unfolding mechanism, irrespective of whether they were monitored by UV absorbance, intrinsic fluorescence, or near-UV CD signal (Fig. 6). Therefore, the heat-induced unfolding process appears

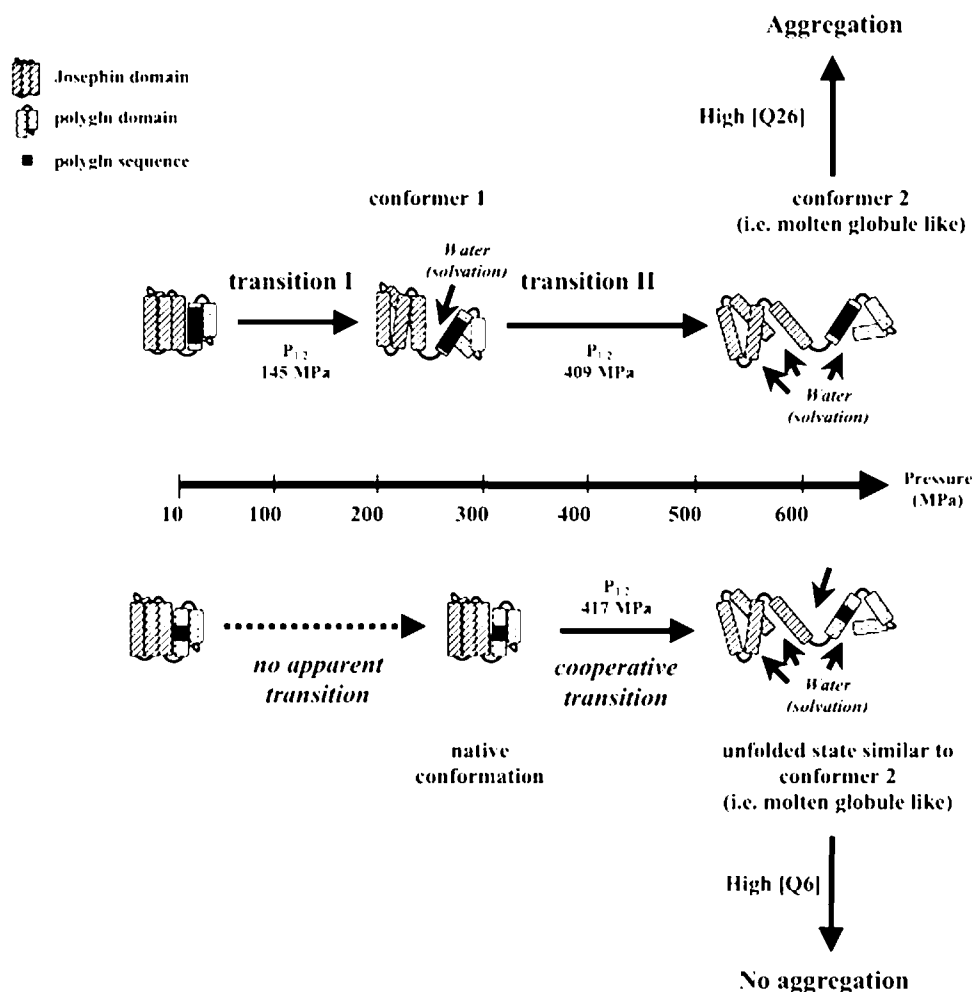


FIG. 10. Schematic representation of the pressure-induced unfolding process for human Q26 and murine Q6 ataxin-3.

to be the same for both proteins despite a lower thermal stability of the murine Q6 as judged by the difference of ΔG_U compared with that of human Q26 (Table I). Furthermore, the possibility to follow the heat-induced unfolding reaction by CD spectroscopy, which is not feasible for technical reasons under pressure (47), provided evidence for the formation of a molten globule-like structure at high temperature; the secondary structure was indeed largely preserved, but the tertiary structure (detected by near-UV CD) collapsed. This is an important observation, as it may provide information about the structural basis of the mechanism of ataxin-3 unfolding (see below). Unlike heat-induced denaturation, pressure-induced unfolding of ataxin-3 was characterized by a complex mechanism, implying several steps and distinct unfolding intermediates within the experimental pressure range. In addition, heat and pressure led to different aggregation mechanisms. Ordered structures were obtained at high pressure, and rather isolated filaments were obtained at high temperature (Fig. 9).

The Glutamine Chain Length as a Negative Determinant of Ataxin-3 Stability—Although human Q26 and murine Q6 ataxin-3 display high sequence homology (Fig. 1) and the same putative three-dimensional folding (18), our spectroscopic data showed significant differences in pressure stability for ataxin-3 orthologues. As shown by fourth derivative spectroscopy and intrinsic fluorescence experiments, the human Q26 started to unfold in a multi-step process at relatively low pressure, whereas the murine Q6 unfolded at pressures higher than 300 MPa. The lower stability of human Q26 was also confirmed by ANS binding experiments. ANS bound to the human protein

above 150 MPa, a pressure similar to the $P_{1/2}$ value of 145 MPa for the first transition observed by UV absorbance and fluorescence (Table I). A similar result was obtained in the presence of 1 M NaCl. Altogether, the results strongly suggest that the lower stability *versus* pressure of human Q26 can be mainly attributed to its longer glutamine chain. Furthermore, human Q26, but not murine Q6, has the propensity to form higher order aggregates by pressure treatment. This process is concentration-dependent and likely follows a nucleation-dependent pathway under pressure as indicated by the observation of aggregates of different structural complexity (Fig. 9). Our result is consistent with the hypothesis that the length of the polyglutamine sequence determines the tendency of ataxin-3 to aggregate, as proposed by Perutz and Windle (10).

Is the Polyglutamine Chain the Only Factor Determining Ataxin-3 Stability and Aggregation?—Several arguments support an additional role of the protein context. Indeed, ataxin-3 can be considered as a two-domain protein: the Josephin domain (18), which contains all three tryptophans and six of eight tyrosines, and the C-terminal, polyGln domain. Therefore, far-UV CD spectroscopy and ANS and ThT binding data are representative of the overall protein structure (comprising the polyglutamine chain), whereas intrinsic fluorescence, UV absorbance, and near-UV CD data reflect the conformational stability of the Josephin domain. For the latter, temperature- and pressure-induced unfolding transitions suggest that the two proteins undergo a similar unfolding process. Actually, similar values of ΔG_U (17.8 *versus* 19.6 $\text{kJ}\cdot\text{mol}^{-1}$) and ΔV (50.5 *versus* 47.1 $\text{ml}\cdot\text{mol}^{-1}$) were obtained from fluorescence data for

the human Q26 and Q6, respectively (Table I). Also, the thermostabilities of human and murine proteins are comparable as indicated by the mid-point temperature values, $t_{1/2}$, of 49.9 and 53.8 °C, respectively. Finally, the most prominent result is that protein aggregation is concomitant with conformational and/or structural changes at high pressure or temperature. Only conformers of human ataxin-3 with solvent exposure of the polyGln domain and partial unfolding of the Josephin domain have the propensity to aggregate. This suggests that the protein environment of the polyGln domain does also play a distinguishing role in the aggregation process of ataxin-3.

Mechanistic Model of Ataxin-3 Unfolding—Our characterization of human Q26 clearly shows that the protein unfolds non-cooperatively (*i.e.* in several steps) under pressure. In the light of the distinct structural changes described above, pressure-induced unfolding of human Q26 can be described as illustrated in Fig. 9. First, applying pressure weakens the interactions between the Josephin and polyGln domains by promoting the entry of water molecules at the interface (transition I). The hydrogen-bonding potential of polar side chain amide groups of glutamine residues favors interactions with water, which reduces protein stabilization through hydrogen-bonded self-interactions (2). The pressure-destabilizing effect induces a partial unfolding of the protein (conformer 1) in which tryptophan residues and hydrophobic regions become more exposed to solvent. Subsequent conformational changes reflect the unfolding process of the Josephin domain (transition II). This transition is mainly characterized by an increased solvent exposure of tryptophan residues. However, the high pressure unfolded state (conformer 2) retains some degree of structure as suggested by ANS binding experiments. This suggests that conformer 2, similar to the heat-induced unfolded protein, resembles a molten globule-like structure, as already observed for several proteins at high pressure (24, 38, 48–51). This conformer binds thioflavin T at high pressure, suggesting that the partly unfolded state of ataxin-3 may form soluble metastable structures, as, for example, pressure-dependent multimers (31, 41). Our hypothesis is reinforced by data obtained in the presence of NaCl. Indeed, salts favor the binding of thioflavin T but not of the ANS probe (Fig. 5). Our interpretation is that NaCl could favor the formation of oligomeric structures at high pressure because of a stabilizing effect of salts, which shields electrostatic interactions at the surface of the protein against pressure unfolding. This effect has also been observed in other systems (52, 53).

In the case of murine protein, the picture is simpler (Fig. 10). The pressure-induced unfolding process is more cooperative. The most likely explanation for the greater stability of murine Q6 under hydrostatic pressure could originate from differences in residue composition of the polyGln domain, most likely the length of the glutamine sequence. Nevertheless, its high pressure unfolded state showed characteristics that were similar to that of conformer 2 of human Q26. This leads to the conclusion of a common unfolding process for both proteins. The critical point that governs the aggregation pathway would be the length of the glutamine expansion.

Biological Relevance—We have shown the greater structural instability of human Q26 relative to murine Q6 and its possible aggregation to higher order structures. A key issue that needs to be addressed is whether the conformational changes leading to aggregation of human Q26 ataxin-3 reflect the early events of SCA3/MJD disease. Perez *et al.* demonstrated that human Q27 ataxin-3 adopts an altered conformation with exposed polyGln domain in the nucleus and binds to the nuclear matrix, a property that has been reported also for the expanded Q78 form (17). Thus, a specific role of the nuclear environment and

more precisely the interactions with nuclear proteins could be the cause of this partial unfolding. Taking into account the preferential recruitment of the protein in the nucleus (12) and its ability to bind transcriptional components (16, 54, 55) one may assume that non-expanded polyGln ataxin-3 could play an important role in aggregation, as already suggested by its presence within neuronal intranuclear inclusions in normal and SCA3/MDJ brains (11). The consequence is that a high concentration of abnormally folded ataxin-3 in specific sub-nuclear domains likely disrupts the biological functions of the nucleus by initiating the oligomerization of proteins and by evolving to aggregates as shown recently (56) for the Q79-hungtintin mutant.

Our results may thus help to understand the early steps of the development of SCA3/MJD. Indeed, we have shown that both exposure of the polyGln domain and partial unfolding of Josephin domain are required for aggregation. In agreement with our observation, Ross *et al.* (57) addressed this issue and proposed a hypothetical pathway in which the polyglutamine fibrillogenesis was preceded by an unfolded state of polyglutamine proteins. Furthermore, our data argue for a dependence of the aggregation process and of the morphology of higher order structured aggregates on the length of the polyGln sequence. This idea is reinforced by the recent work of Tortora and co-workers (19) who showed that non-pathological human ataxin-3 carrying 36 glutamines could form β -fibrils at high temperature.² Perez *et al.* (17) have also observed that the non-pathological ataxin-3 adopts an altered conformation in the nucleus where the polyGln domain is exposed. Our results may well explain these observations, in that they suggest that the protein has a rigid and virtually undenaturable scaffold consisting of secondary structure elements, along with a flexible, overall tertiary structure. Thus, these properties might represent the structural prerequisites that explain the capability of human ataxin-3 to modify its conformation without undergoing denaturation as a result of interactions with well defined molecular partners found in the nucleus.

Acknowledgments—We are indebted to Christian Valentin for efficient technical help. We are grateful to J. A. and J. Kornblatt (Concordia University) and more particularly Dr. C. Balny for valuable discussions and for correcting the manuscript.

REFERENCES

- Paulson, H. L., Perez, M. K., Trotter, Y., Trojanowski, J. Q., Subramony, S. H., Das, S. S., Vig, P., Mandel, J. L., Fischbeck, K. H., and Pittman, R. N. (1997) *Neuron* **19**, 333–344
- Perutz, M. F., Johnson, T., Suzuki, M., and Finch, J. T. (1994) *Proc. Natl. Acad. Sci. U. S. A.* **91**, 5355–5358
- Thakur, A. K., and Wetzel, R. (2002) *Proc. Natl. Acad. Sci. U. S. A.* **99**, 17014–17019
- Paulson, H. L., Das, S. S., Crino, P. B., Perez, M. K., Patel, S. C., Gotsdiner, D., Fischbeck, K. H., and Pittman, R. N. (1997) *Ann. Neurol.* **41**, 453–462
- Zoghbi, H. Y., and Orr, H. T. (2000) *Annu. Rev. Neurosci.* **23**, 217–247
- Cummings, C. J., and Zoghbi, H. Y. (2000) *Annu. Rev. Genomics Hum. Genet.* **1**, 281–328
- Bevino, A. E., and Loll, P. J. (2001) *Proc. Natl. Acad. Sci. U. S. A.* **98**, 11955–11960
- Orr, H. T. (2001) *Genes Dev.* **15**, 925–932
- Orr, H. T. (2001) *Lancet* **358**, Suppl. 1, S35
- Perutz, M. F., and Windle, A. H. (2001) *Nature* **412**, 143–144
- Fujigasaki, H., Uchihara, T., Koyano, S., Iwabuchi, K., Yagishita, S., Makifuchi, T., Nakamura, A., Ishida, K., Toru, S., Hirai, S., Ishikawa, K., Tanabe, T., and Mizusawa, H. (2000) *Exp. Neurol.* **165**, 248–256
- Fujigasaki, H., Uchihara, T., Takahashi, J., Matsushita, H., Nakamura, A., Koyano, S., Iwabuchi, K., Hirai, S., and Mizusawa, H. (2001) *J. Neurol. Neurosurg. Psychiatry* **71**, 518–520
- Kettner, M., Willwohl, D., Hubbard, G. B., Rub, U., Dick, E. J., Jr., Cox, A. B., Trotter, Y., Auburger, G., Braak, H., and Schultz, C. (2002) *Exp. Neurol.* **176**, 117–121
- Ono, S., Inoue, K., Mannen, T., Mitake, S., Shirai, T., Kanda, F., Jinnai, K., and Takahashi, K. (1989) *Acta Neuropathol.* **77**, 350–356
- Tatton, N. A. (2000) *Exp. Neurol.* **166**, 29–43

² E. Shehi, P. Fusi, F. Secundo, S. Pozzuolo, A. Bairata, and P. Tortora, unpublished observations.

16. Chai, Y., Wu, L., Griffin, J. D., and Paulson, H. L. (2001) *J. Biol. Chem.* **276**, 44889–44897
17. Perez, M. K., Paulson, H. L., and Pittman, R. N. (1999) *Hum. Mol. Genet.* **8**, 2377–2385
18. Albrecht, M., Hoffmann, D., Evert, B. O., Schmitt, I., Wullner, U., and Lengauer, T. (2003) *Proteins* **50**, 355–370
19. Mombelli, E., Afshar, M., Fusi, P., Mariani, M., Tortora, P., Connelly, J. P., and Lange, R. (1997) *Biochemistry* **36**, 8733–8742
20. Mozhaev, V. V., Heremans, K., Frank, J., Masson, P., and Balny, C. (1996) *Proteins* **24**, 81–91
21. Goldsteins, G., Andersson, K., Olofsson, A., Dacklin, I., Edvinsson, A., Baranov, V., Sandgren, O., Thylen, C., Hammarstrom, S., and Lundgren, E. (1997) *Biochemistry* **36**, 5346–5352
22. Torrent, J., Connelly, J. P., Coll, M. G., Ribo, M., Lange, R., and Vilanova, M. (1999) *Biochemistry* **38**, 15952–15961
23. Ruan, K., Lange, R., Zhou, Y., and Balny, C. (1998) *Biochem. Biophys. Res. Commun.* **249**, 844–848
24. Ruan, K., Lange, R., Meersman, F., Heremans, K., and Balny, C. (1999) *Eur. J. Biochem.* **265**, 79–85
25. Ferrao-Gonzales, A. D., Souto, S. O., Silva, J. L., and Foguel, D. (2000) *Proc. Natl. Acad. Sci. U. S. A.* **97**, 6445–6450
26. Roitel, O., Bec, N., Lange, R., Balny, C., and Branlant, G. (2001) *Biochem. Biophys. Res. Commun.* **283**, 347–350
27. Silva, J. L., Foguel, D., and Royer, C. A. (2001) *Trends Biochem. Sci.* **26**, 612–618
28. Perrett, S., and Zhou, J. M. (2002) *Biochim. Biophys. Acta* **1595**, 210–223
29. Kuwata, K., Li, H., Yamada, H., Legname, G., Prusiner, S. B., Akasaka, K., and James, T. L. (2002) *Biochemistry* **41**, 12277–12283
30. Balny, C., Masson, P., and Heremans, K. (2002) *Biochim. Biophys. Acta* **1595**, 3–10
31. Torrent, J., Alvarez-Martinez, M. T., Heitz, F., Liautard, J. P., Balny, C., and Lange, R. (2003) *Biochemistry* **42**, 1318–1325
32. Lange, R., Frank, J., Saldana, J.-L., and Balny, C. (1996) *Eur. Biophys. J.* **24**, 277–283
33. Lange, R., Bec, N., Mozhaev, V. V., and Frank, J. (1996) *Eur. Biophys. J.* **24**, 284–292
34. King, L., and Weber, G. (1986) *Biochemistry* **25**, 3637–3640
35. Silva, J. L., Miles, E. W., and Weber, G. (1986) *Biochemistry* **25**, 5780–5786
36. Ruan, K., and Weber, G. (1989) *Biochemistry* **28**, 2144–2153
37. Nandi, P. K., Leclerc, E., and Marc, D. (2002) *Biochemistry* **41**, 11017–11024
38. Ruan, K., Lange, R., Bec, N., and Balny, C. (1997) *Biochem. Biophys. Res. Commun.* **239**, 150–154
39. Ruan, K., Xu, C., Yu, Y., Li, J., Lange, R., Bec, N., and Balny, C. (2001) *Eur. J. Biochem.* **268**, 2742–2750
40. LeVine, H., III (1999) *Methods Enzymol.* **309**, 274–284
41. Carrotta, R., Bauer, R., Waninge, R., and Rischel, C. (2001) *Protein Sci.* **10**, 1312–1318
42. Cummings, C. J., and Zoghbi, H. Y. (2000) *Hum. Mol. Genet.* **9**, 909–916
43. Lakowicz, J. R. (1983) *Principles of Fluorescence Spectroscopy*, Plenum Press, New York
44. Ruan, K., Tian, S., Lange, R., and Balny, C. (2000) *Biochem. Biophys. Res. Commun.* **269**, 681–686
45. Zhang, J., Peng, X., Jonas, A., and Jonas, J. (1995) *Biochemistry* **34**, 8631–8641
46. Chatani, E., Nonomura, K., Hayashi, R., Balny, C., and Lange, R. (2002) *Biochemistry* **41**, 4567–4574
47. Balny, C., Lange, R., Heitz, F., Connelly, J. P., Saldana, J.-L., and Ruan, K. (1998) *Rev. High Pressure Sci. Technol.* **7**, 1292–1296
48. Kobashigawa, Y., Sakurai, M., and Nitta, K. (1999) *Protein Sci.* **8**, 2765–2772
49. Peng, X., Jonas, J., and Silva, J. L. (1993) *Proc. Natl. Acad. Sci. U. S. A.* **90**, 1776–1780
50. St John, R. J., Carpenter, J. F., Balny, C., and Randolph, T. W. (2001) *J. Biol. Chem.* **276**, 46856–46863
51. Vidugiris, G. J., and Royer, C. A. (1998) *Biophys. J.* **75**, 463–470
52. Bancel, F., Bec, N., Ebel, C., and Lange, R. (1997) *Eur. J. Biochem.* **250**, 276–285
53. Kornblatt, J. A., and Hoa, G. H. (1990) *Biochemistry* **29**, 9370–9376
54. Chai, Y., Shao, J., Miller, V. M., Williams, A., and Paulson, H. L. (2002) *Proc. Natl. Acad. Sci. U. S. A.* **99**, 9310–9315
55. Li, F., Macfarlan, T., Pittman, R. N., and Chakravarti, D. (2002) *J. Biol. Chem.* **277**, 45004–45012
56. Sanchez, I., Mahlke, C., and Yuan, J. (2003) *Nature* **421**, 373–379
57. Ross, C. A., Poirier, M. A., Wanker, E. E., and Amzel, M. (2003) *Proc. Natl. Acad. Sci. U. S. A.* **100**, 1–3

**Structural Instability and Fibrillar Aggregation of Non-expanded Human Ataxin-3
Revealed under High Pressure and Temperature**

Stéphane Marchal, Erlet Shehi, Marie-Cécile Harricane, Paola Fusi, Frédéric Heitz, Paolo Tortora and Reinhard Lange

J. Biol. Chem. 2003, 278:31554-31563.

doi: 10.1074/jbc.M304205200 originally published online May 23, 2003

Access the most updated version of this article at doi: [10.1074/jbc.M304205200](https://doi.org/10.1074/jbc.M304205200)

Alerts:

- [When this article is cited](#)
- [When a correction for this article is posted](#)

[Click here](#) to choose from all of JBC's e-mail alerts

This article cites 55 references, 12 of which can be accessed free at <http://www.jbc.org/content/278/34/31554.full.html#ref-list-1>